# Piezoelectric sensing and non-parametric statistical signal processing for health monitoring of hysteretic dampers used in seismic-resistant structures

A. Gallego [a,*], A. Benavent-Climent [b], L. Romo-Melo [a]

[a] Department of Applied Physics, Granada University, Spain
[b] Department of Structural Mechanics, Granada University, Spain

*Keywords:*
Hysteretic damper
Vibration tests
Time series analysis
Health monitoring
Power spectral density
Frequency response function

A B S T R A C T

The paper proposes a new application of non-parametric statistical processing of signals recorded from vibration tests for damage detection and evaluation on I-section steel segments. The steel segments investigated constitute the energy dissipating part of a new type of hysteretic damper that is used for passive control of buildings and civil engineering structures subjected to earthquake-type dynamic loadings. Two I-section steel segments with different levels of damage were instrumented with piezoceramic sensors and subjected to controlled white noise random vibrations. The signals recorded during the tests were processed using two non-parametric methods (the power spectral density method and the frequency response function method) that had never previously been applied to hysteretic dampers. The appropriateness of these methods for quantifying the level of damage on the I-shape steel segments is validated experimentally. Based on the results of the random vibrations, the paper proposes a new index that predicts the level of damage and the proximity of failure of the hysteretic damper.

## 1. Introduction

The traditional seismic design approach relies on the inelastic deformation of particular zones of the structure to dissipate most of the energy input by an earthquake (commonly, beam-ends and column-ends on moment-resisting frames). In contrast, in structural control systems, this energy is delivered to special devices that can be repaired or replaced after suffering damage. This is one of the reasons why structural control systems are installed on civil or building structures to improve their response under seismic events or wind loads and mitigate risks. In general terms, structural control systems can be classified into three categories: active, hybrid and passive. Active control systems consist of real-time processing sensors and force delivery devices that require an external source of power. Hybrid control systems use minimal power to change the control force opposed by certain elements of the structure. Although active and hybrid control are very powerful techniques, their application is normally restricted to large or very singular

* Corresponding author.
*E-mail addresses:* antolino@urg.es (A. Gallego), benavent@ugr.es (A. Benavent-Climent), lyrome@ugr.es (L. Romo-Melo).

structures. In contrast, passive control systems consist of energy-dissipating devices (dampers) that do not require any external source of power.

Passive control systems afford many advantages: (i) the inelastic deformations are concentrated in the seismic dampers, and the damage in the parent structure can be drastically reduced or eliminated; (ii) the addition of damping reduces the lateral displacements of the structure, which also reduces damage to non-structural elements; (iii) by strategically locating the seismic dampers, their inspection, repair and/or replacement following an earthquake can be carried out with minimal cost and without interrupting occupancy. Overall, passive control systems are more affordable and can be more easily implemented in general purpose structures. These technologies have been increasingly taken into consideration in the USA after the Northridge earthquake (1994). Likewise, since the Kobe (1995) earthquake in Japan, more buildings have been designed to include dampers [1,2].

A structure with passive control comprises a main frame designed to predominantly sustain the gravity loads, and a series of special energy dissipating devices (EDD) also called dampers, which dissipate most of the energy input by the earthquake, as shown in Fig. 1.

Several mechanisms have been used for passive energy dissipation, including metal yielding, phase transformation of metals, friction sliding, fluid orificing, viscous dampers, deformation of viscoelastic solids or liquids [3–5] and hysteretic dampers [6]. Viscous (solid or liquid) and friction dampers dissipate the vibration energy through heat, while hysteretic dampers are based on the yielding or phase transformation of metals. The hysteretic damper is one of the most widely used EDDs due to its good balance between cost and efficiency. However, since both yield and phase transformation of metals involve inelastic strains in the material (i.e. damage), evaluating the health of the hysteretic damper after a seismic event is a matter of great concern.

The goal of passive control systems is to limit the damage on the main structure under different levels of ground motion hazard. In the modern framework of seismic design called performance based design, the level of damage allowed on the main structure for each level of seismic hazard must be determined by the designer. For minor or moderate earthquakes (i.e. those with a probability of exceedance of 50% and 20% in 50 years), the main frame of a structure with hysteretic EDDs must remain within the elastic range (i.e. undamaged) and most of the seismic input energy must be dissipated through plastic deformations on the EDDs. Wind storms can also induce plastic deformations on the dampers while the main frame remains within the elastic range. Minor to moderate earthquakes and wind storms can occur several times during the lifetime of structure and usually do not exhaust the energy dissipation capacity of the hysteretic EDD. That is, the EDDs would not need to be replaced after a minor or moderate earthquake or after a wind storm, provided that their health (i.e. level of damage) and their proximity to failure can be reliably evaluated. Simple visual inspection is not enough to determine the proximity to failure of a hysteretic EDD because the damage caused by the plastic deformation of the steel is not visible until the element is in its final stage, near collapse.

Non-destructive techniques (NDT) or structural health monitoring (SHM) strategies can be appropriate to determine whether the hysteretic EDDS need to be replaced after a seismic event or wind storm. SHM refers to systems embedded in the structure that may detect the occurrence of damage that represents a structural risk. This saves time and reduces maintenance costs because unnecessary inspections and replacements are avoided. In contrast to NDT, SHM strategies assume that sensors are permanently attached to the structure, working for its whole service life without operator intervention. Thus, data collected by the sensors that are distributed throughout the structure must be automatically processed and synthesized for warning signals when damage is detected.

In recent years, many SHM techniques have been improved and new sensor technologies have appeared in the area of damage detection in structures. The goal of these innovations is that the structures can be self-sensed and intelligent, to preserve their integrity, optimize their performance, and provide continuous safety for their users and operators. Most experiments are oriented toward aeronautical and civil areas, and are applied to composite materials, aircraft structures, aluminium plates, glass fiber panels and reinforced concrete columns and blocks.

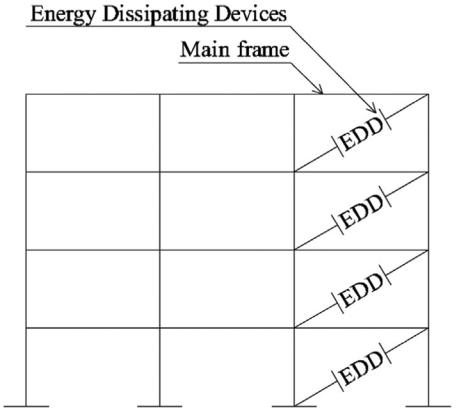


**Fig. 1.** Basic configuration of a frame with energy dissipating devices (EDD).

Traditional sensor technologies for SHM systems include piezoelectric, accelerator or ultrasonic sensors. Moreover, new sensor technologies have also been developed, mainly intended for the actuation or deformation of adaptive elements or structures [7]. These include active fiber sensors [8,7], smart nanoscale materials and carbon nanotubes (CNT) [9], smart aggregate or multi-functional piezoceramic-based devices [10] and embedded piezoelectric-wafer active sensors [11,12]. Although many of these technologies are accurate and robust, most of them are expensive or require a high computational cost. The choice of sensor technology depends on the characteristics of the system under study.

The main reason behind using piezoelectric sensors (PZTs) for capturing the vibration responses at both high and low frequency ranges is their low cost. In ordinary buildings provided with hysteretic EDDs, using SHM systems with expensive devices (such as accelerators) cannot be justified because a type of action such as an earthquake has a very low probability of occurrence. In contrast, PZTs are able to produce and receive vibration signals of sufficient quality (ruggedness and sensitivity) within the small area of interest where the damage is generated on the EDD, while furthermore ensuring that the global measurement system, permanently installed on the dampers, maintains its low cost. In other words, although the PZT elements present a performance in capturing vibration responses that is poorer than other instruments such as accelerators, they prove much cheaper and good enough to provide a robust estimation of the level of damage on the hysteretic dampers.

A number of studies for damage detection and estimation are based on changes in natural frequencies of the structure, while other more sophisticated methods are based on elastic wave propagation [8,12,13], electro-mechanical (E/M) impedance [12] or guided waves [11] to identify reflections and changes in the transmission phase/velocity of the signals through the structure. Most of these techniques use piezoelectric sensors to acquire the signals proving that there is a strong correlation between the presence and size of damage and the character of signals transmitted by the piezoelectric sensor (vibration-based fault detection) [14]. These variations can be detected and evaluated using a proper processing of signals and correlated with presence (Level 1 in SHM), position (Level 2 in SHM) and intensity of damage (Level 3 in SHM).

There are plenty of papers in the literature dealing with time vibration series analysis for damage detection in structures and materials [14–16] but to date none of these techniques had been applied to evaluate the level of damage on hysteretic EDDs.

The use of model-based methods of frequency obtained from a simple vibration signal can be very appropriate for specific applications like this. These methods use direct measurement of the frequency response [17], analysis of its characteristics [18], differences between frequency representations [19] and compressed models of frequency [20], in order to obtain feasible indicators of structural damage from in situ measurements, without exhaustive analysis. Deriving frequency representations such as power spectral density (PSD) or frequency response function (FRF) from vibration signals is not a difficult task. These methods are straightforward [21] and do not require many sensors to provide real information regarding the structural dynamic behavior [22]. The principal advantage of vibration signals is that they can be acquired quickly [23]. Frequency variables such as PSD and FRF are moreover the easiest to obtain in real time, which is why faster and cheaper damage detection methods can be implemented from them.

In this respect, a research project underway at the University of Granada (Spain) [24] aims to develop and validate a robust SHM system for hysteretic EDDs installed in frame structures for earthquake protection. Two key elements are involved in this objective. One is to develop a permanent and economic system of sensors on the EDD capable of recording key physical variables that would inform about their response during the earthquake. The second facet consists of implementing algorithms of low computational cost to detect and identify changes in the response of the EDD that are sensitive to the presence and to the level of damage.

This paper presents an experimental study on a practical SHM system designed for a particular type of hysteretic EDD consisting of short segments of I-shape steel sections assembled in such a way that energy is dissipated through out-of-plane plastic strains on the web of the I-shape steel segments [25]. The assemblage of the I-shape steel segments that dissipate the energy and the auxiliary elements is referred to hereafter as web plasticization damper (WPD). The paper proposes a new application of non-parametric statistical processing of signals recorded with this SHM system from vibration tests conducted on the I-section steel segments to detect and evaluate the level of damage. To this end, I-section with different levels of damage were instrumented with piezoceramic sensors and subjected to controlled white noise random vibrations. The signals recorded during the tests were analyzed by using two non-parametric methods [15] (power spectral density frequency response function) never previously applied to hysteretic dampers, and their suitability was validated experimentally. These frequency-domain non-parametric methods are based on quantitative comparisons between the vibration response of an inspected EDD (for which the presence of damage is not known) and the vibration response of a healthy EDD used as baseline. The methods incorporate a statistical test for deciding whether the EDD is damaged or not damaged (Level 1 in SHM) with a previously assumed level of risk. Level 2 of SHM (i.e. localization) is not relevant in this particular application because the damage is concentrated on the EDD, which are small in size and located in well-identified places of the frame. However, Level 3 of SHM must be attained in this particular application, because determining the capability of the dampers to protect the structure against future earthquakes is of paramount importance. The paper also proposes a new index of damage based on the results of random vibrations to predict the level of damage and the proximity of failure of the hysteretic damper.

The application of non-parametric statistical processing signals recorded from vibration tests to the evaluation of damage in hysteretic dampers and the proposal of a new index, called the Area Index Damage, are two original contributions of this work.

## 2. Test specimens and setup

The WPD is a brace-type structural element which is intended to be used in moment resisting frames as a conventional diagonal or bracing member (see Fig. 1) [25]. The WPD is an assemblage of short segments of wide-flange or I-shape steel sections which constitute the EED, and two auxiliary steel elements that connect the EDD to two diagonally opposite beam-column joints of the frame, as shown in Fig. 2. The assemblage is arranged in such a way that when the WPD is subjected to forced deformations in the axial direction, the web of the wide-flange or I-shape section undergoes out-of-plane flexural deformations.

These short segments of wide-flange or I-sections constitute a simple and inexpensive EDD, as minimum manufacturing is required and leftovers that are not useful for other structural purposes can be re-utilized.

In this experimental study, EDDs consisting of 90 mm length segments of I-shape steel sections (test specimen) are investigated, isolated from the auxiliary elements as shown in Fig. 3. The EDD are cut from a single bar of structural wide-flange section of $140 \times 75$ mm (total depth flange width), referred to as IPE-140 hereafter. Under expected working conditions, the deformation pattern of the EDD is as shown in Fig. 4. Under out-of-plane flexural deformations, the plastic strains (i.e. the damage) would be concentrated at the edges of the web near the flanges, as indicated by the shaded region in Fig. 4. Under repeated cycles of deformation, the plastic strain concentration in these regions results in small cracks that progressively reduce the effective thickness of the web in its connection with the flange, leading to the failure of the EDD.

In order to simulate the aforementioned reduction of effective width of the web near the connections with the flanges in laboratory-controlled conditions, two short segments of I-shaped sections, hereafter called specimens A1 and A2, were sawed consecutively with four different depths in the connection of web and flanges to represent four different levels of damage: $D_1$, $D_2$, $D_3$, and $D_4$.

Fig. 5 shows the remaining width $t_r$ of the web after the saw cutting. Table 1 summarizes the values of $t_r$ for each level of damage, the latter expressed by the ratio $100 \times (t - t_r)/t$, where $t$ is the initial width of the web. The healthy or undamaged specimen used as the base line is called $D_o$. In the severest level of damage, $D_4$, the EDD was on the brim of breaking.

The boundary conditions of the web of the I-shape steel section when it is assembled with the auxiliary elements to form the WPD and subjected to axial loading is clamped–clamped. These boundary conditions were reproduced in the setup shown in Fig. 6, where both flanges of the I-section are prevented from displacing and rotating.

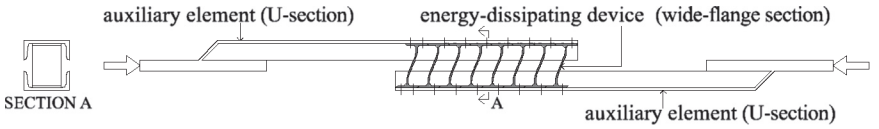


**Fig. 2.** Detail of the web plastifying damper.

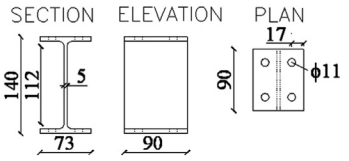


**Fig. 3.** Test specimen: short length segments of I-shape steel sections (dimensions in mm).

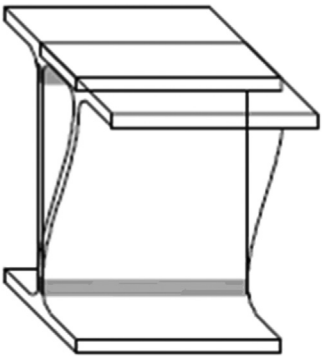

**Fig. 4.** Deformation pattern of the I-shape steel section.

## 3. Vibration tests for damage detection

After each level of damage ($D_1$, $D_2$, $D_3$, and $D_4$) was induced on the web of the I-section steel segment by saw cutting, vibration tests were carried out to detect the presence of damage and evaluate its intensity. Each test involved exciting the web of the I-section through a controlled vibration signal, $x[t]$, and simultaneously recording the response, $y[t]$, at four points of the web as shown in Fig. 7a.

The web was excited with a PZT sensor that served as actuator (see Fig. 7b), and the response was measured with four PZT sensors glued on the opposite side of the web and denoted $s1$, $s2$, $s3$ and $s4$ in Fig. 7c. The signals recorded by these sensors are referred to as $y_i[t]$ $(i: 1-4)$ hereafter. The vibration tests were carried out with the specimen mounted on the setup shown in Fig. 6.

PI®PRYY+0220 wrapped piezoelectric ceramic sensors were used both as PZT actuator and PZT sensors. The frequency response of these PZT sensors shows an almost flat behavior in the bandwidth [0.3–20] kHz, as seen in Fig. 8.

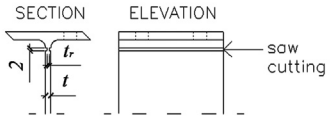


**Fig. 5.** Saw cutting (dimensions in mm).

**Table 1**
Levels of damage induced in specimens A1 and A2.

| Damage level | $t_r$ (mm) | % Damage |
|---|---|---|
| $D_0$ | 5 | 0 |
| $D_1$ | 4 | 20 |
| $D_2$ | 3 | 40 |
| $D_3$ | 2 | 60 |
| $D_4$ | 1 | 80 |

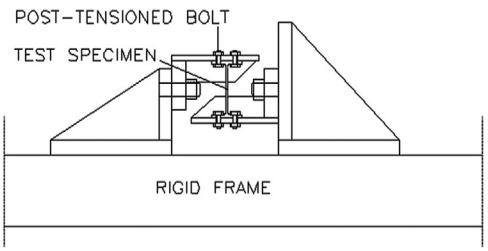


**Fig. 6.** Experimental setup.

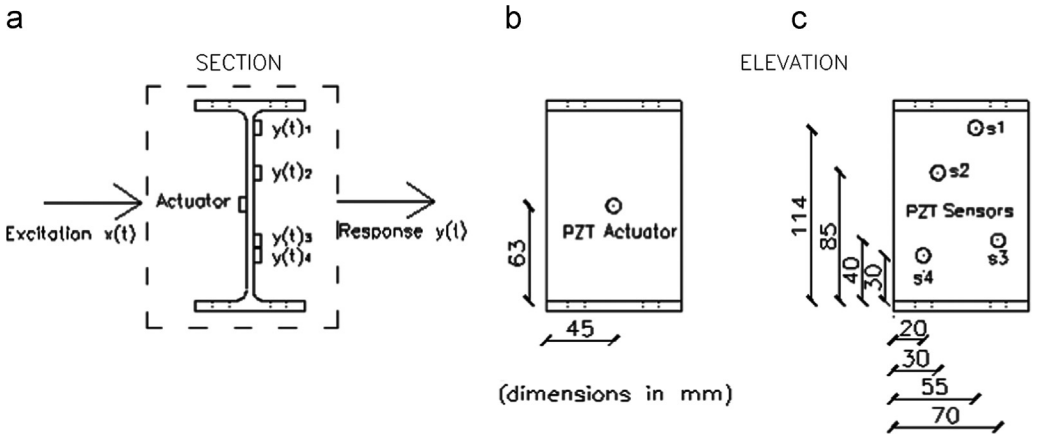


**Fig. 7.** (a) Section view of specimen, (b) frontal view with actuator position, and (c) frontal view with position of sensors.

As can be seen in Fig. 8, the frequency bandwidth selected for this study ([0.3–20] kHz) is within the flat zone of the sensor frequency response. Thus, the resonant peaks and nonlinearities pertaining to the sensor do not have any influence on the analysis carried out here. This plot was obtained from a PZT excited by a white noise signal, with another similar PZT attached to the first one (see [26] for details).

Brüel&Kjær PULSE equipment was used both as the signal generator of the random excitation $x[t]$ and as the acquisition system to record the response vibration signals $y_i[t]$. The PULSE system provides an output signal with a maximum peak about 5 V, which was seen to be insufficient for properly exciting the specimen; therefore, a gain $G=20$ was used. In addition, to ensure a good quality of the signals, the acquisition system was configured in the differential mode, i.e. two channels of the PULSE equipment were used for each PZT sensor, one on each of its two electrodes. This configuration made it possible to measure the signal of each PZT as the difference between the two channels, thus avoiding any reference to the electric ground. Moreover, to avoid both mechanical and electric noise, a ground system was installed throughout the cable network and connected to an embedded mass system that was independent of the ground system of the laboratory building. A complete scheme of generation and measurement equipment can be seen in Fig. 9.

Vibration tests were carried out using a white noise signal excitation $x[t]$ in the 0.1 Hz–25.6 kHz bandwidth (BW). For both $x[t]$ and $y[t]$ signals, the sampling frequency used was $f_s=65{,}536$ Hz, which corresponds to a sampling period of $\Delta t = 1.5 \times 10^{-5}$ s.

The total number $N$ of data recorded was $N=196{,}608$, corresponding to 3 s of acquisition time duration. For statistical reasons, five vibration tests were carried out for each level of damage ($D_0$, $D_1$, $D_2$, $D_3$, and $D_4$) and for each specimen, using

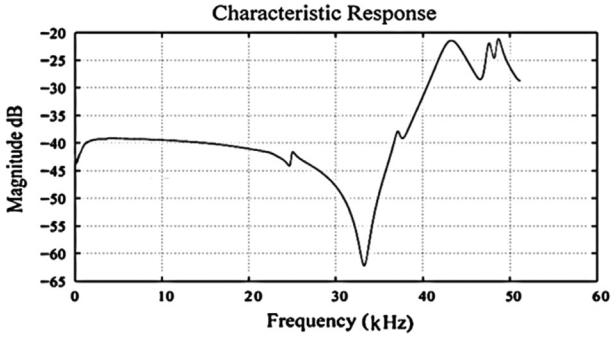


**Fig. 8.** Frequency response of the PZT sensors and actuator used.

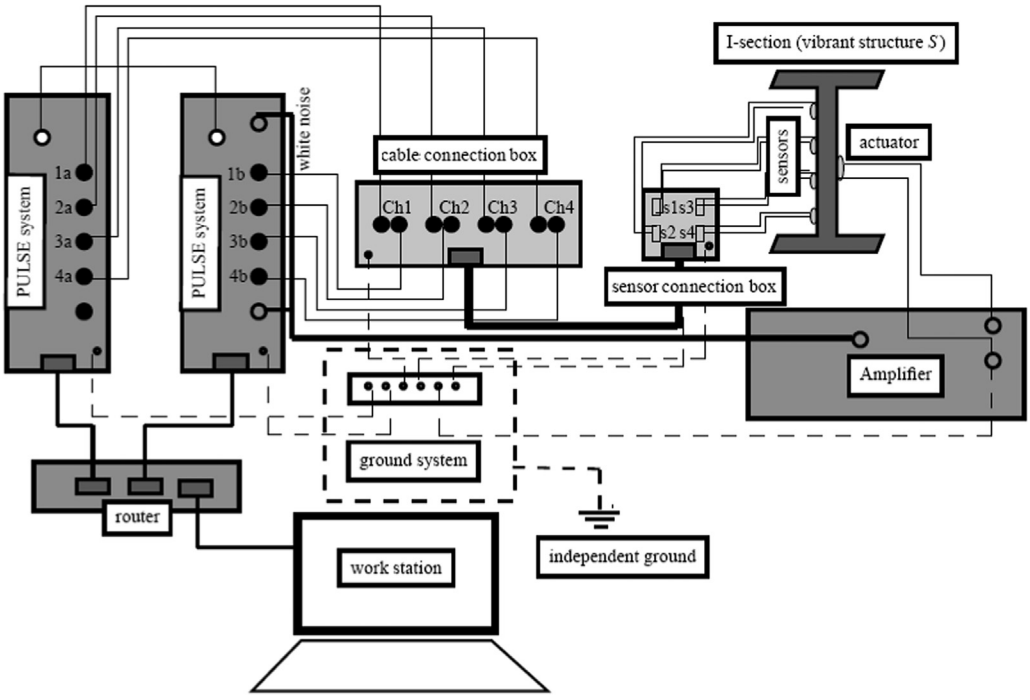


**Fig. 9.** Equipment scheme for vibration tests.

a different white noise sequence in each but maintaining the same frequency content. After the tests, the signals were suitably pre-processed for data conditioning purposes. This pre-processing consisted of the following steps:

- *Filtering:* A BW=[0.3–20] kHz pass-band filter was applied to prevent some electrical noise and possible nonlinear performance of sensors. Finite element numerical simulations conducted prior to the tests confirmed that at least 17 natural frequencies of the specimen were located inside the frequency range [0.3–20] kHz, which proved to be enough for damage detection and evaluation purposes.
- *Normalization and scaling:* For numerical reasons, in order to counteract different excitation levels and environmental conditions, and in order to compensate the off-set and amplitude variability among signals, the following normalization process was applied:

$$x[t]_n = \frac{x[t]-\overline{x}[t]}{\sigma(x[t])}; \quad y[t]_n = \frac{y[t]-\overline{y}[t]}{\sigma(y[t])} \tag{1}$$

where $x[t]_n$ and $y[t]_n$ are the normalized signals ($t = 1\Delta t, 2\Delta t, \ldots N\Delta t$), $\overline{x}[t]$ and $\overline{y}[t]$ are their mean values, and $\sigma(x[t])$ and $\sigma(y[t])$ their standard deviation, respectively. For the sake of simplicity, from now on the simpler notation $x[t]$ and $y[t]$ will be used for the normalized signal $x[t]_n$ and $y[t]_n$, i.e. $x[t] \equiv x[t]_n$, $y[t] \equiv y[t]_n$. Thus, after acquisition and signal conditioning, vibration data recorded for each specimen were collected into a vector named $z[t] = [x[t], y[t]]^T$.

## 4. Damage assessment

When applying vibration time-series methods for damage detection, it is assumed that the inspected specimen (named $S_u$) is a linear time-invariant (LTI) system, deterministic and stationary system [15,27], as shown in Fig. 10.

The first goal is to assess the damage of $S_u$ until Level 1 in SHM, i.e., to ascertain whether this specimen is damaged or not. It is a decision between two options or hypotheses designated as $H_o$ (the inspected specimen is undamaged $S_o$), and its opposite, $H_1$ (the inspected specimen is damaged) [15], that is

$$H_o: S_u = S_o: \text{ null hypothesis (undamaged specimen)} \tag{2}$$

$$H_1: S_u \neq S_o: \text{ alternative hypothesis (damaged specimen)} \tag{3}$$

This decision is made on the basis of the value of a feature quantity, $Q$, which has to be sensitive to the presence of damage. $Q$ is "estimated" from the vibration data set $z[t]$ following the procedure shown in Fig. 11, which includes a baseline phase and inspection phases.

First (baseline phase), a baseline is formed using the available data from the undamaged specimen $S_o$. Its vibration response $z_o[t]$ must be known from previous vibration tests or from numerical simulations. Thus, using $z_o[t]$, the feature quantity $\hat{Q}_o$ corresponding to the undamaged specimen is obtained. Second (inspection phase), vibration tests are conducted with the inspected specimen to obtain the response $z_u[t]$, and the corresponding feature quantity $\hat{Q}_u$. Then, the statistical hypothesis testing is done by comparing $\hat{Q}_u$ with its counterpart $\hat{Q}_o$ to decide whether the specimen is damaged or healthy. The definition of $\hat{Q}$ and the statistical tests are explained in the next section.

## 5. Non-parametric methods for damage feature definition and statistical hypothesis testing

In contrast to parametric methods that call for previous knowledge of data distribution, non-parametric methods are inferential procedures that do not assume a fixed model structure [15,28]. Owing to their simplicity and fewer underlying assumptions, their application is widespread and robust. This study uses two non-parametric models already used in the past: (i) the power spectral density (PSD) method which uses only the response signals $y[t]$; and (ii) the frequency response function (FRF) method, which uses both excitation and response signals contained in the vector $z[t] = [x[t], y[t]]^T$. The physical base of both procedures is the shift in the frequency response produced by the damage [15,16,27]. The non-parametric models (PSD and FRF) are estimated from the available data $z[t] = [x[t], y[t]]^T$. Ideally, these estimators are consistent, that is, $\hat{Q}$ and $Q$ are close (with little deviation) to the true PSD and FRF.

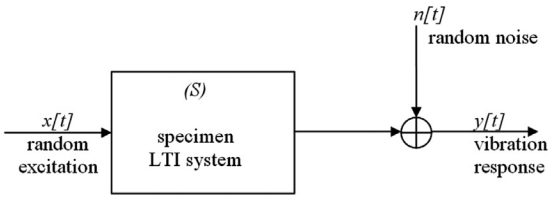


**Fig. 10.** Linear time-invariant system with additive response noise.

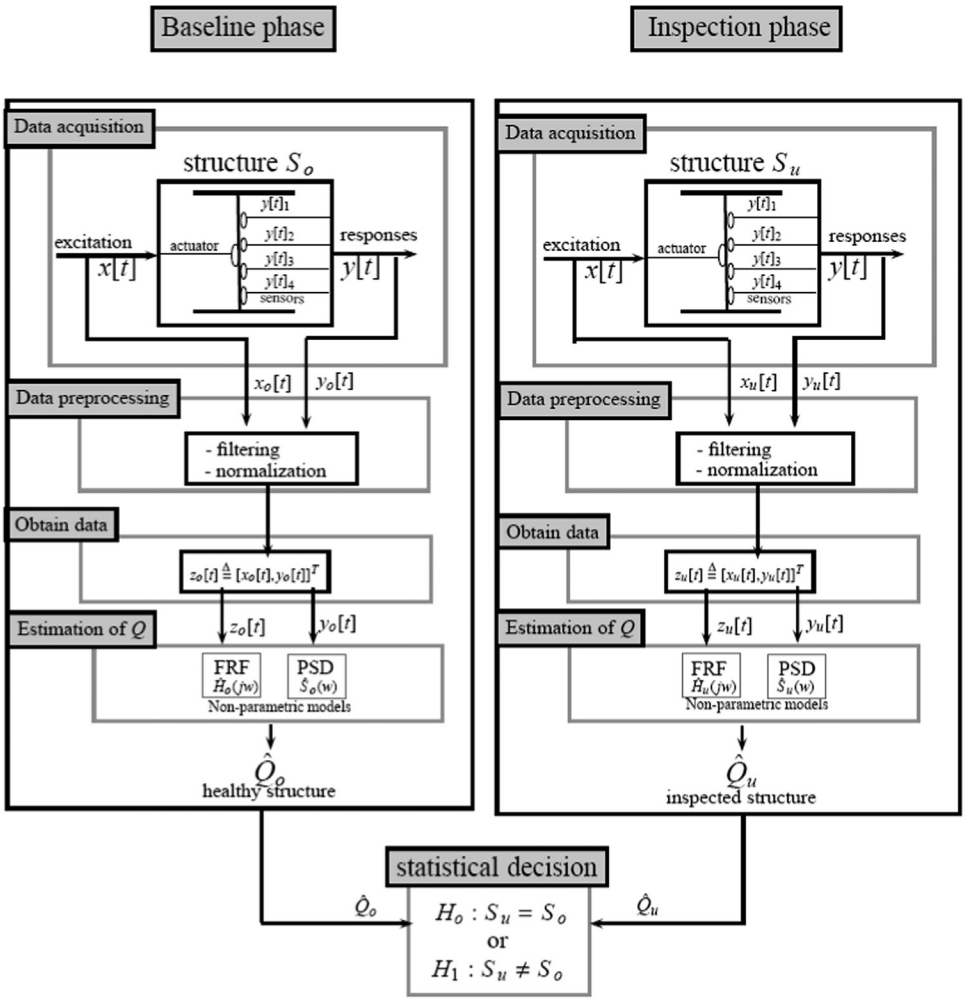


**Fig. 11.** Damage detection scheme using two different statistical non-parametric methods.

### 5.1. *The power spectral density based method*

This method uses the PSD of the response signals obtained with the Welch estimator to obtain the feature quantity estimate $\hat{Q}$ [15], i.e.

$$\hat{Q}_{PSD} = \hat{Y}(\omega) = \frac{1}{K}\sum_{k=1}^{K}\frac{1}{N}\left|\sum_{t=1}^{N} a[t]\cdot y[t]^{(k)}\cdot e^{-j\omega t\Delta t}\right|^2 \tag{4}$$

where $\omega$ is the angular frequency, $K$ is the number of segments in which $y[t]$ is divided, $a[t]$ represents the function used for signal windowing, and the subscript $k$ represents the $k$th segment. This estimator, normalized by the true power spectral density, $Y(\omega)$, and multiplied by $2K$, is statistically characterized by a central Chi-square distribution with $2K$ degrees of freedom, $\chi^2(2K)$ [15], i.e.

$$\frac{2K\cdot\hat{Y}(\omega)}{Y(\omega)} \sim \chi^2(2K) \tag{5}$$

The hypothesis testing is established as

$$H_o: Y_o(\omega) = Y_u(\omega) \quad \text{and} \quad H_1: Y_o(\omega) \neq Y_u(\omega) \tag{6}$$

Damage detection is based on whether there is statistically significant deviation between the healthy specimen $S_o$ and the inspected specimen $S_u$ in the PSD function. The $F$-statistic relating the Welch PSD estimates of the undamaged specimen,

$\hat{Y}_o(\omega)$, with the inspected one, $\hat{Y}_u(\omega)$, is constructed as follows:

$$F = \frac{2K \cdot \hat{Y}_o(\omega)/Y_o(\omega)}{2K \cdot \hat{Y}_u(\omega)/Y_u(\omega)} \tag{7}$$

Under the assumption that the null hypothesis ($H_o: Y_o(\omega) = Y_u(\omega)$) is true (healthy specimen) the $F$-statistic can be simplified as follows:

$$F = \frac{\hat{Y}_o(\omega)}{\hat{Y}_u(\omega)} \tag{8}$$

The distribution of the $F$-statistic (Eq. (8)) is shown in Fig. 12a. From this distribution a proper choice between $H_o$ and $H_1$ can be made. $1-\alpha$ is the confidence interval and $\alpha$ is the so-called risk level assumed. If $F$ remains within the confidence interval, the null hypothesis $H_o$ must be accepted, and then, the inspected specimen will be considered as undamaged with a certainty of 95%. Otherwise, the alternative hypothesis $H_1$ will be accepted, and the specimen will be considered as damaged.

### 5.2. *The frequency response function based method*

This method uses the FRF magnitude estimate from the signals $x[t]$ and $y[t]$ to obtain the feature quantity $\hat{Q}$ [15], i.e.

$$\hat{Q}_{FRF} = \left|\hat{H}(j\omega)\right| = \frac{\left|\widehat{XY}(j\omega)\right|}{\hat{X}(\omega)} \tag{9}$$

where $\widehat{XY}(j\omega)$ and $\hat{X}(\omega)$ are the cross- and auto-spectral density functions of the signals $x[t]$ and $y[t]$, respectively, estimated using the Welch estimator [15]. It can be demonstrated that this quantity is statistically characterized by a normal distribution whose mean value is the true FRF magnitude, $|H(j\omega)|$, and a variance $\sigma^2(\omega)$ [15]. The hypothesis testing is established as follows:

$$H_o: |H_o(j\omega)| - |H_u(j\omega)| = 0 \quad \text{and} \quad H_1: |H_o(j\omega)| - |H_u(j\omega)| \neq 0 \tag{10}$$

In this case, damage detection is based on confirmation of statistically significant deviations (from the healthy $S_o$) in the inspected specimen FRF function at some frequencies, through a hypothesis-testing problem. The statistic that relates the undamaged specimen with the inspected one is constructed as follows:

$$\delta\left|\hat{H}(j\omega)\right| = \left|\hat{H}_o(j\omega)\right| - \left|\hat{H}_u(j\omega)\right| \sim N(\delta|H(jw)|, \delta\sigma^2(\omega)) \tag{11}$$

Under the assumption that the null hypothesis is true $H_o: \delta|H(j\omega)| = 0$ and $\delta\sigma^2(\omega) = \sigma_o^2(\omega) + \sigma_o^2(\omega) = 2\sigma_o^2(\omega)$, i.e. the statistic has a normal distribution $\delta\left|\hat{H}(j\omega)\right| \sim N(0, 2\sigma_o^2(\omega))$. Then, the $Z$-statistic can be normalized as

$$Z = \frac{\delta\left|\hat{H}(j\omega)\right|}{\sqrt{2\hat{\sigma}_o^2(\omega)}} \tag{12}$$

The standard normal distribution of the $Z$-statistic (Eq. (12)) is shown in Fig. 12b. From this distribution a proper selection between $H_o$ and $H_1$ can be made. If $Z$ remains within the confidence interval, $|Z| \leq Z_{1-\alpha/2}$, the null hypothesis $H_o$ must be accepted, and then, the inspected specimen will be considered as undamaged with a certainty of 95%. Otherwise, the alternative hypothesis $H_1$ will be accepted, and the specimen will be considered as damaged. $Z_{1-(\alpha/2)}$ is the standard normal

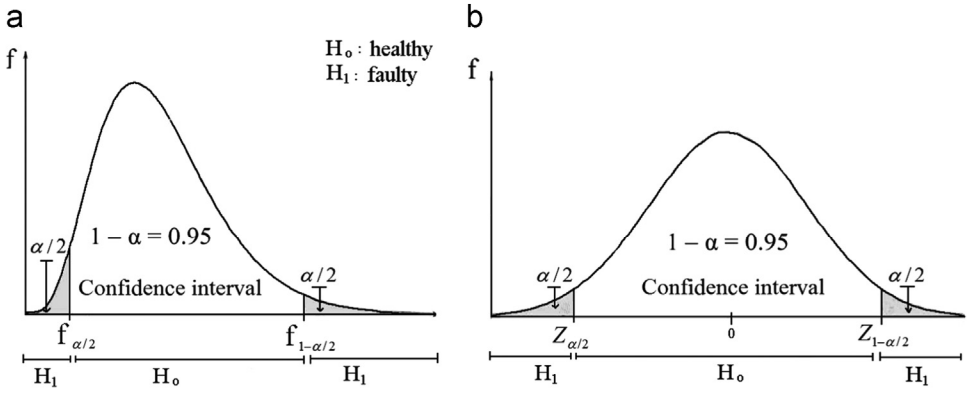


**Fig. 12.** Probability density of $F$-statistic (a) and $Z$-statistic (b) under $|H_o|$.

distribution's $1-(\alpha/2)$ critical point, which has typical values $\alpha=0.05$ and $Z_{1-(\alpha/2)}=1.96$ [15]. The selection of the appropriate level of risk must take into account that (1) the main decision to be taken in light of the results of the SHM procedure is whether it is necessary or not to change the energy dissipators (i.e. the I-section steel segments) after an earthquake; and (2) the behaviour of the main structure in the event of future earthquakes depends largely on the "health" of the energy dissipators, for which reason they must be considered as primary elements of a building's earthquake resistant system.

In both methods, the statistic test and the risk level can be represented in terms of the frequency, with the spectra and the horizontal line shown in Fig. 13. If the entire spectrum of the statistic is below the horizontal line representing the risk level (Fig. 13a), the specimen is considered to be healthy with 95% $(1-\alpha=0.95)$ of certainty. Otherwise, if some peak of the spectra crosses the horizontal line (Fig. 13b), the specimen is considered damaged. If the inspected specimen is damaged (i.e. hypothesis $H_1$) it is reasonable to assume that: the larger the area delimited by the spectrum of the statistic above the risk level, (i.e. shaded area in Fig. 13b), the higher the level of damage. Accordingly, the following damage index AID (Area Index Damage) is proposed here to evaluate the intensity of the damage (Level 3 in SHM)

$$\mathrm{AID}=\int_{\omega_{\min}}^{\omega_{\max}}\xi(\omega)\,d\omega,\quad \forall\xi(\omega)\geq\alpha \tag{13}$$

where $\xi(\omega)$ represents either the $F$-statistic or the $|Z|$-statistic.

## 6. Experimental results

The I-section steel segments referred to as specimens A1 and A2 in Section 2 were instrumented as explained in Section 3. In addition to the undamaged level, four levels of artificial damage were performed for each specimen as explained in Section 2 by sawing the edges of the web. For the undamaged level and for each level of artificial damage, five vibration tests were carried out on each specimen.

For illustrative purposes, Fig. 14a shows the response signal of the undamaged specimen A1 measured with the sensor $s2$, $y_2[t]$.

The experiments showed that the PZT sensors, used as actuators under a white noise signal, are able to excite all frequency components of the system with equal power intensity. Further, the PZT allowed us to capture the vibration response signals with the quality necessary for such an application. We should stress that this approach is designed to cover very small areas, and amplitude-signal losses are insignificant.

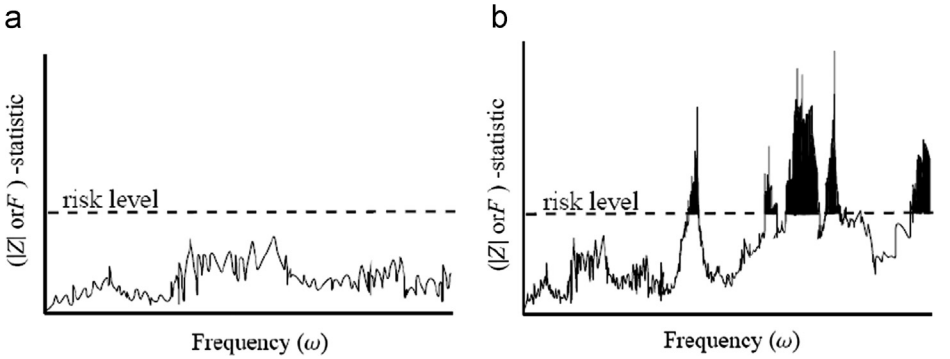


**Fig. 13.** Graphic representation of the statistical test. (a) Healthy structure and (b) faulty structure.

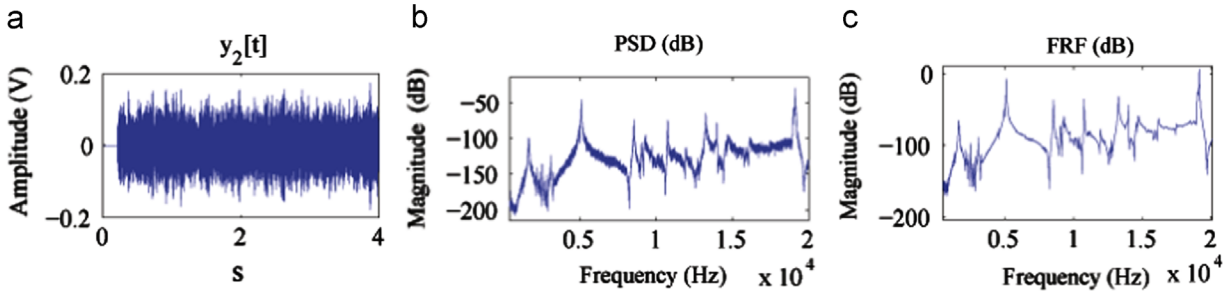


**Fig. 14.** Undamaged specimen A1 ($D_0$) at sensor 2. (a) Response signal $y_2[t]$. (b) Welch based PSD estimate. (c) Welch based FRF magnitude estimate.

Fig. 14b shows the magnitude of PSD (in decibels), estimated with Eq. (4), of the vibration signals obtained from sensor s2 and the undamaged specimen A1. Fig. 14c shows the Welch based FRF magnitude estimate with Eq. (9). The amplitude of the response signal was similar (about 150 mV) for the four sensor positions, i.e. the position of sensor hardly affected the peak voltage amplitude in vibration signals. As seen in Fig. 14c, the magnitude of the FRF estimate shows the frequency response without the spurious effects of white noise excitation, which allows the resonances of the specimen and the frequency shifts attributable to damage to be clearly detected.

The spectral density of the feature quantity $\hat{Q}_{FRF}$ of the signals in the bandwidth [0.3–20] kHz was obtained for all levels of damage ($D_1$, $D_2$, $D_3$, and $D_4$) and compared with the corresponding spectrum for the undamaged specimen ($D_0$). This comparison was carried out for the four sensors $s1$, $s2$, $s3$ and $s4$ and for both specimens, A1 and A2.

Fig. 15 shows the results obtained from sensor $s2$ for both specimens. It is clear for both specimens that, as expected, damage produces a significant frequency shift of the $\hat{Q}_{FRF}$ spectrum. Also, the degree of shift of the spectrum towards the left side is seen to increase consistently with the increased level of damage.

Fig. 16 shows six different bandwidths of the $\hat{Q}_{FRF}$ spectra in which the resonance peaks are more sensitive to the presence of damage: $BW_1$=[1–2], $BW_2$=[4–6], $BW_3$=[7–9], $BW_4$=[10–11], $BW_5$=[12.3–13.7] and $BW_6$=[18.5–19.5] kHz. These bands were selected for the posterior application of statistical analysis. A zoom display of these bands is shown in Fig. 17. A more detailed inspection of the bandwidth $BW_2$=[4–6] kHz, shown in Fig. 18, indicates that the resonant peak shifts towards the left side about 60 Hz for each level of damage, from about 5079 Hz for the undamaged specimen $D_0$ to 4848 Hz for level of damage $D_4$.

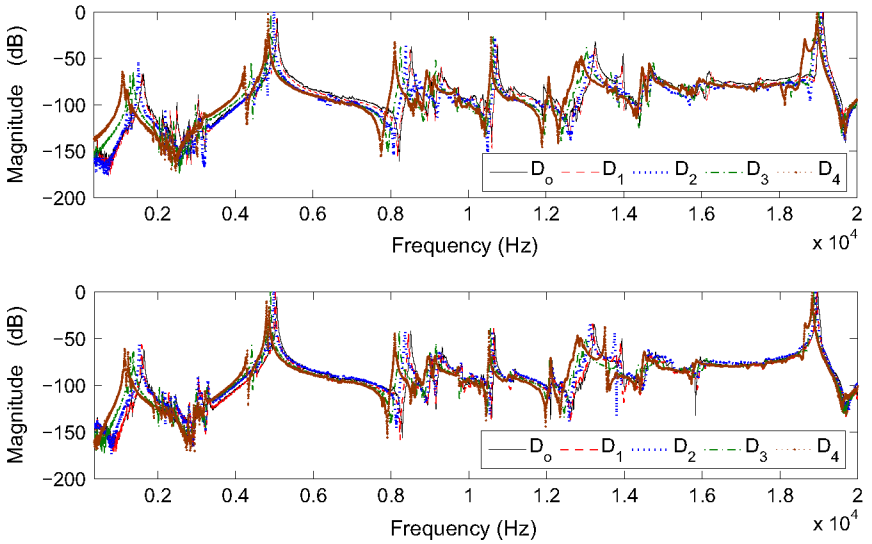


**Fig. 15.** $\hat{Q}_{FRF}$ spectra for the undamaged and for the four damage levels obtained from sensor $s2$. Top: specimen A1. Bottom: specimen A2.

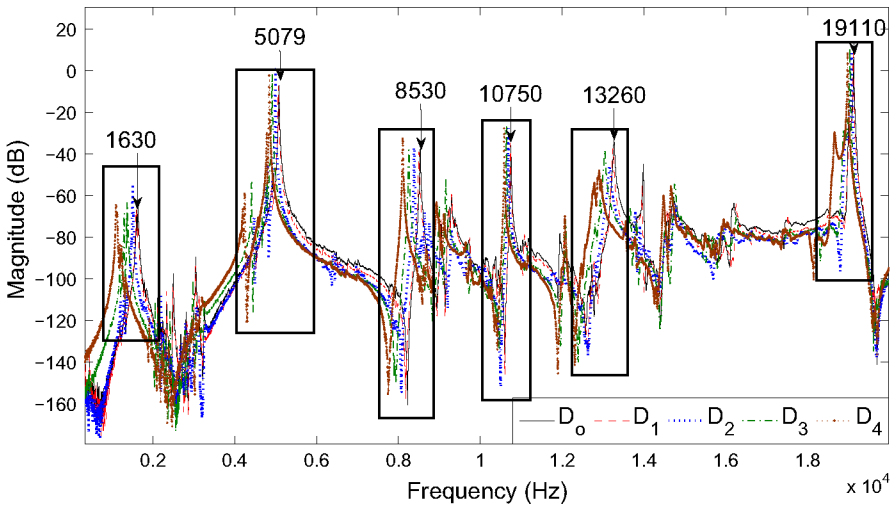


**Fig. 16.** Relevant bandwidths of the $\hat{Q}_{FRF}$ spectra obtained from sensor $s2$ of specimen A1.

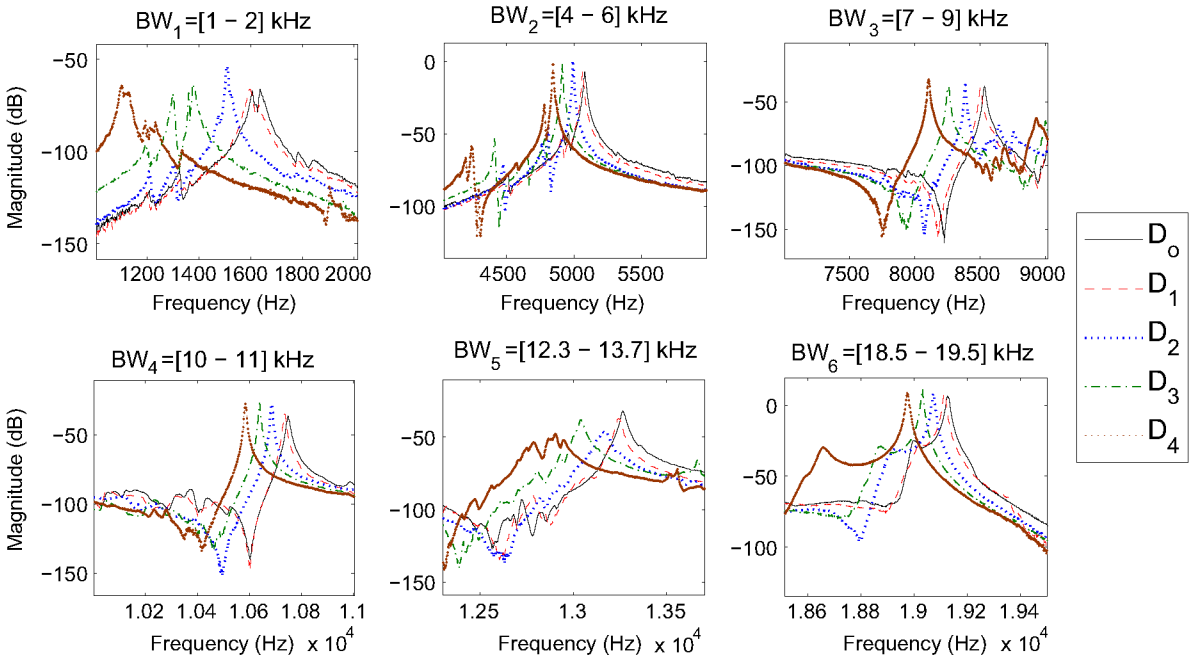


**Fig. 17.** Frequency bands of the $\hat{Q}_{FRF}$ spectra obtained from sensor *s*2 of specimen A1.

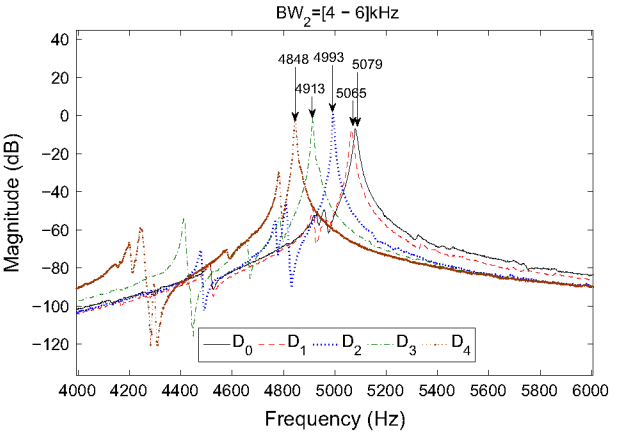


**Fig. 18.** $\hat{Q}_{FRF}$ for all levels of damage ($D_0 - D_4$). Specimen A1, Sensor 2 and $BW_2$=[4–6] kHz.

The statistical tests presented in Section 4 were applied separately to each bandwidth $BW_1$–$BW_6$, both for the $\hat{Q}_{PSD}$ and for the $\hat{Q}_{FRF}$ spectra, using a risk limit $\alpha = 0.05$. As an example, Fig. 19 shows the statistical tests based on the PSD and FRF method obtained for specimen A1 with the signal of sensor 2 and using the bandwidth $BW_2$. It can be clearly seen that the area enveloped by the curve above the horizontal line that determines the risk level increases as the level of damage increases. This area determines the damage index AID defined in Section 5.

The consistent increase of this area with the actual level of damage induced on the specimen suggests that AID provides a quantitative measure of the level of damage on the inspected specimen. This fact is confirmed by plotting the values of AID against the level of damage, as shown in Fig. 20. Since the first damage level $D_1$ was very slight, only one peak slightly crossed the threshold line and the resulting AID for $D_1$ was close to zero.

Fig. 21 shows the two AIDs calculated with the statistical test, based on PSD and on FRF methods, from the signals obtained with the four sensors in the same bandwidth $BW_2$=[4–6] kHz. Although the range of values of AID varies with the position of the sensor and the feature used (PSD or FRF), in all cases there is an approximately linear relationship between AID and the level of damage. For a given bandwidth, the different ranges of values of AID depending on the position of the sensor can be attributed to its proximity to nodes or antinodes of the vibration mode whose frequency is associated with the band frequency.

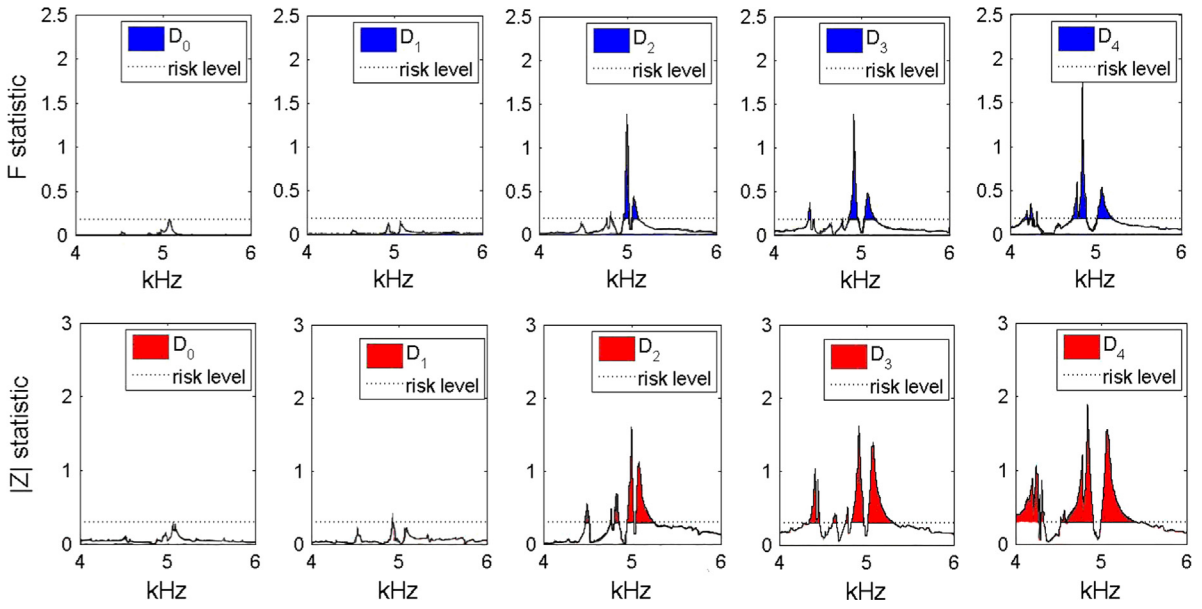


**Fig. 19.** Application of the statistical tests based on the PSD (top) and FRF (bottom) methods to all the specimens with different levels of damage ($D_0 - D_4$). Specimen A1, Sensor 2 and $BW_2 = [4–6]$ kHz.

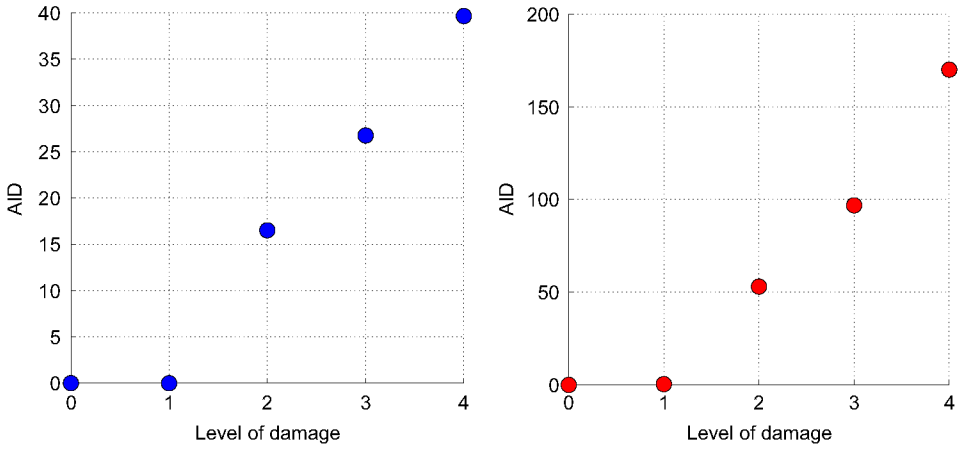


**Fig. 20.** AID obtained for specimen A1 from sensor *s*2 in the bandwidth $BW_2 = [4–6]$ kHz, based on the PSD method (left) and on the FRF method (right).

According to Fig. 21, for bandwidth $BW_2$, sensor 3 is located in the position most sensitive to damage since it presents the largest range of AID values. If the position of a sensor is close to a node of a vibration mode associated with a given frequency $\omega_i$, this sensor can hardly capture the level of damage in the bandwidth around $\omega_i$ [29].

Finally, Figs. 23 and 24 show the values of AID obtained for the six bandwidths of frequency selected in Fig. 16. Fig. 22 corresponds to specimen A1 and Fig. 23 to specimen A2. These results corroborate the aforementioned observation that the AID value varies with the choice of the frequency band used for its calculation.

## 7. Concluding remarks

A new application entailing the non-parametric statistical processing of signals recorded from white noise input vibration tests for damage detection, with evaluation on I-section steel segments, is proposed in this paper. The steel segments constitute the energy dissipating part of a new type of hysteretic damper that is used for passive control of buildings and civil engineering structures subjected to earthquake-type dynamic loadings. The vibration signals recorded on I-section steel segments with piezoceramic sensors subjected to different levels of damage were processed by means of two non-parametric based methods (power spectral density and frequency response function), experimentally validating the appropriateness of these methods for quantifying the level of damage on the I-section steel segments. The new index (AID) proposed here, defined as the area delimited by the spectral curve above the assumed risk level, was tested by comparing it with the artificial

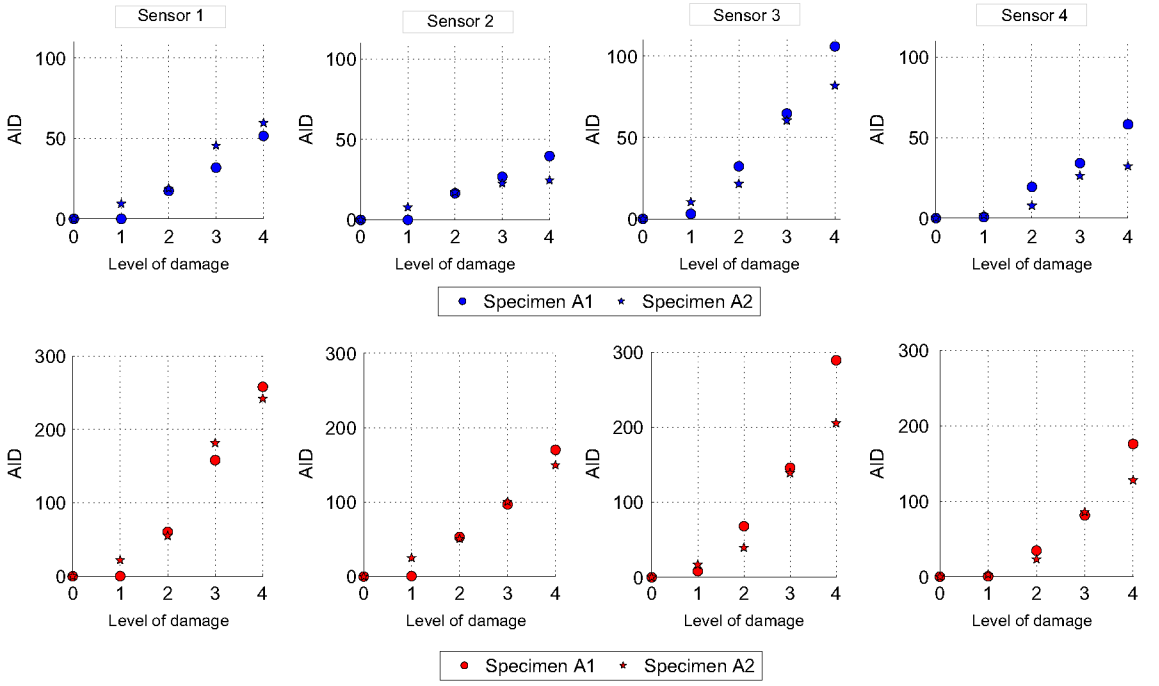


**Fig. 21.** Area Damage Index (AID) based on the PSD (top) and on the FRF (bottom) method for all position sensors. Specimen A1 (circular mark) and specimen A2 (star mark), Sensor 2. Bandwidth $BW_2$=[4–6] kHz.

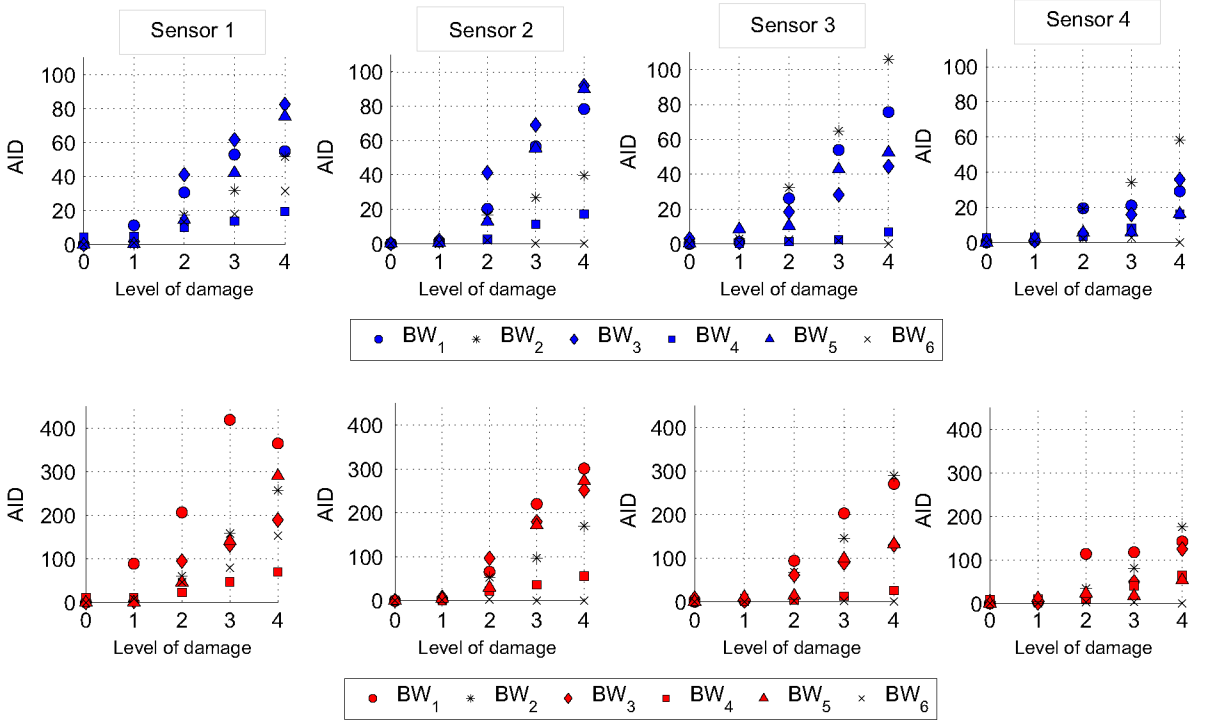


**Fig. 22.** Area Damage Index (AID) based on the PSD (top) and FRF (bottom) for specimen A1. Frequency bands $BW_1$=[1–2], $BW_2$=[4–6], $BW_3$=[7–9], $BW_4$=[10–11], $BW_5$=[12.3–13.7] and $BW_6$=[18.5–19.5] kHz.

damage level induced on the specimens. Its behaviour, seen to vary depending on the damage level, the sensor position and the frequency range used, is detailed in this paper for two similar specimens, revealing that (i) a very good correlation is seen between the AID and the real level of damage, and its sensitivity to the level of damage makes it suitable for future SHM real

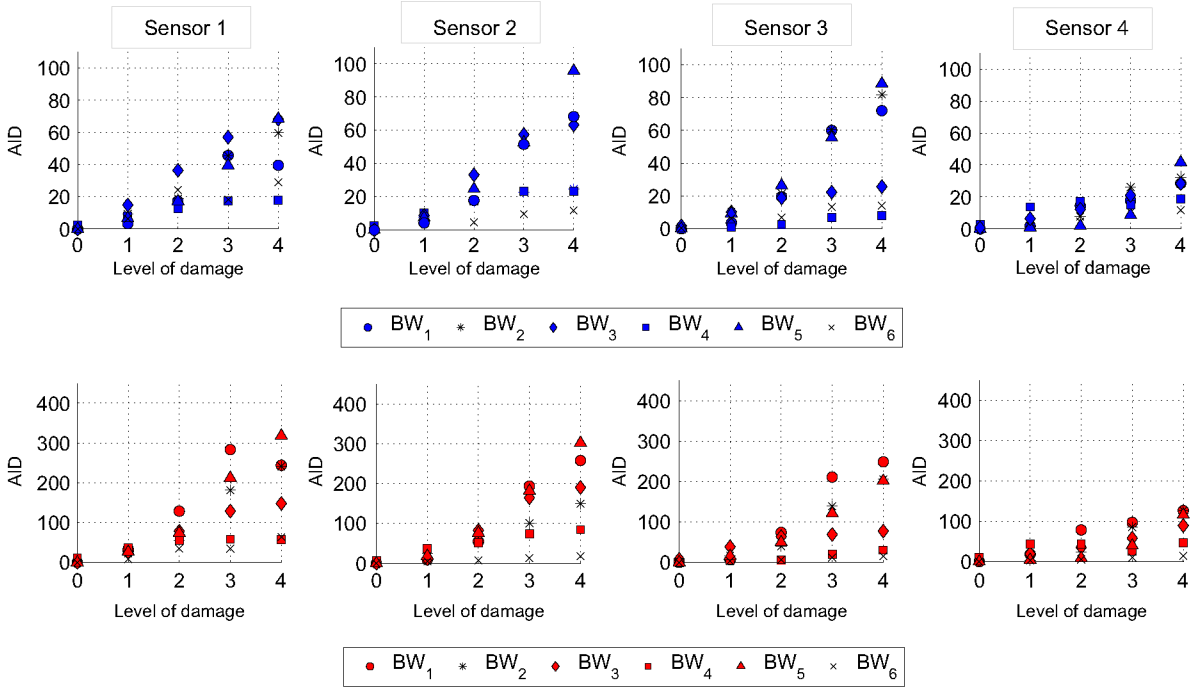


**Fig. 23.** Area Damage Index (AID) based on the PSD (top) and FRF (bottom) for specimen A2. Frequency bands $BW_1$=[1–2], $BW_2$=[4–6], $BW_3$=[7–9], $BW_4$=[10–11], $BW_5$=[12.3–13.7] and $BW_6$=[18.5–19.5] kHz.

applications; (ii) there is a natural dependence on the position of the sensor and the frequency range used; (iii) the sensing and measuring equipment and setup provide high robustness against mechanical and electromagnetic noise.

For the application investigated in this paper, the location of the damage was not a concern because damage always develops at the ends of the web of the I-section steel segments that constitute the energy dissipators. In addition, small levels of damage are not a concern because they do not imply replacing the energy dissipators. The authors believe that the proposed approach can be applied in the future to other structural elements for which small amounts of damage could be an issue. Also, in future research the authors intend to correlate the results described here with other innovative techniques and approaches based on modal analysis, stress wave propagation techniques or electro-mechanical impedance, which are being widely studied and developed for new applications in recent years.

The main contribution of the proposed damage index (AID) is that it allows for estimation of damage to dampers by means of simple vibration tests, maintaining the low cost of the instrumented damper while providing a diagnosis in real time. Also, AID can be correlated with more accurate damage indices which are not appropriate for real application to seismic-resistant designs because they entail expensive instrumentation and costly computational processes.

These results are a firm first step in the development and validation of a robust SHM system for hysteretic EDDs to be installed in frame structures for seismic protection.

## Acknowledgments

This research received the financial support of the local government of Spain, Consejería de Innovación, Ciencia y Tecnología, Projects P07-TEP-02610 and P08-TEP-03641. The authors also appreciate the collaboration of Andrés Roldán-Aranda and Leandro Morillas for their help in the experimental setup, and the orientation by Prof. Fassois during the short term stay of Liliana Romo at the University of Patras (Greece), on the subject of non-parametric methods for SHM.

## References

[1] A. Wada, Y. Huang, M. Iwata, Passive damping technology for building in Japan, Prog. Struct. Eng. Mater. 2 (3) (2000) 335–350.
[2] M. Symans, F. Charney, A. Whittaker, M. Constantinou, C. Kircher, Energy dissipation systems for seismic applications: current practice and recent developments, J. Struct. Eng. 134 (1) (2008) 3–21.
[3] P. Boardman, B. Wood, A. Carr, Union house—a cross braced structure with energy dissipaters, Bull. N. Z. Natl. Soc. Earthq. Eng. 16 (2) (1983) 63–75.
[4] E. Martines-Romero, Experiences on the use of supplementary energy dissipators on building structures, Earthq. Spectra 9 (3) (1993) 581–625.
[5] C. Perry, E. Fierro, H. Sedarat, R. Scholl, Seismic upgrade in San Francisco using energy dissipation devices, Earthq. Spectra 9 (3) (1993) 559–579.
[6] M.D. Symans, F.A. Charney, A.S. Whittaker, M.C. Constantinou, C.A. Kircher, M.W. Johnson, R.J. McNamara, Energy dissipation systems for seismic applications: current practice and recent developments, J. Struct. Eng.—ASCE 134 (1) (2008) 3–21.

[7] A. Brunner, M. Barbezat, C. Huber, P. Flueler, The potential of active fiber composites made from piezoelectric fibers for actuating and sensing applications in structural health monitoring, Mater. Struct. 38 (2005) 561–567.
[8] G. Kirikera, S. Datta, M. Schulz, A. Ghoshal, M. Sundaresan, J. Feaster, D. Hughes, Recent advances in an artificial neural system for structural health monitoring, in: Proceedings of the SPIE 5046, Nondestructive Evaluation and Health Monitoring of Aerospace Materials and Composites II, San Diego, CA, 2003.
[9] P. Kang, M. Schulz, J. Lee, G. Choi, J. Jung, J. Choi, S. Hwang, A carbon nanotube smart material for structural health monitoring, J. Solid State Phenom. 120 (2006) 289–296.
[10] H. Gu, Y. Moslehy, D. Sanders, G. Song, Y. Mo, Multi-functional smart aggregate-based structural health monitoring of circular reinforced concrete columns subjected to seismic excitations, Smart Mater. Struct. (19) (2010) 1–8.
[11] V. Giurgiutiu, Lamb wave generation with piezoelectric wafer active sensors for structural health monitoring, in: 10th Annual International Symposium on Smart Structures and Materials and Eighth Annual International Symposium on NDE for Health Monitoring and Diagnostics, San Diego, CA, 2002.
[12] V. Giurgiutiu, A. Zagrai, J. Bao, Piezoelectric wafer embedded active sensors for aging aircraft structural health monitoring, Struct. Health Monitor. J. 1 (1) (2002) 41–61.
[13] G. Kawiecki, Piezogenerated elastic waves for structural health monitoring smart structures, in: Smart Structures, Kluwer Academic Publishers, Dordrecht, The Netherlands, 1999, pp. 133–142.
[14] K. Worden, D. Manson, Experimental validation of a structural health monitoring methodology: Part.1. Novelty detection on a laboratory structure, J. Sound Vib. 259 (2) (2003) 323–343.
[15] S. Fassois, J. Sakellariou, Time series methods for fault detection and identification in vibrating structures, R. Soc.—Philos. Trans.: Math. Phys. Eng. Sci. (365) (2006) 411–448.
[16] F. Kopsaftopoulos, S. Fassois, Vibration based health monitoring for a thin aluminum plate—a comparative assessment of statistical time series methods, in: Proceedings of the Fifth European Workshop on Structural Health Monitoring (EWSHM), Sorrento, Italy, 2010.
[17] R. Sampaio, N. Maia, J. Silva, Damage detection using the frequency–response–function curvature method, J. Sound Vib. 226 (5) (1999) 1029–1042.
[18] I. Trendafilova, W. Heylen, Categorization and pattern recognition methods for damage localization from vibration measurements, Mech. Syst. Signal Process. 17 (4) (2003) 825–836.
[19] Y. Ni, X. Zhou, J. Ko, Experimental investigation of seismic damage identification using pca-compressed frequency response functions and neural networks, J. Sound Vib. 290 (1–2) (2006) 242–263.
[20] C. Zang, M. Imregun, Structural damage detection using artificial neural networks and measured frf data reduced via principal component projection, J. Sound Vib. 242 (5) (2001) 813–827.
[21] R. Bandara, T. Chan, D. Thambiratnam, Frequency response function based structural damage detection using artificial neural networks, in: International Conference on Structural Engineering, Construction and Management, Sri Lanka, 2001.
[22] A. Choudhury, Damage detection in structures using measured frequency response function data (Ph.D. Thesis), Victoria University of Technology, Melbourne, Australia, 1996.
[23] O. Salawu, Detection of structural damage through changes in frequency: a review, Eng. Struct. 19 (9) (1997) 718–723.
[24] A. Benavent-Climent, Desarrollo e implementación de la tecnología de los disipadores de energía aplicada al control del daño en construcciones sometidas a terremotos, y su evaluación mediante técnicas avanzadas de tratamiento de señales, Proyecto de Investigación de Excelencia. Consejería de Innovación, Ciencia y Empresa. Junta de Andalucía, 2007.
[25] A. Benavent-Climent, L. Morillas, J.M. Vico, A study on using wide-flange section web under out-of-plane flexure for passive energy dissipation, Earthq. Eng. Struct. Dyn. 40 (5) (2011) 473–490.
[26] L. Romo-Melo, Health monitoring of health monitoring of wpd-type hysteretic dampers used for passive control of earthquake resistant structures by means of vibration analysis in the frequency domain (Ph.D. Thesis), University of Granada, Spain, 2012.
[27] S. Fassois, Statistical Time Series Methods for Structural Health Monitoring, Advanced Course on Structural Health Monitoring, University of Patras, Greece, April 2009.
[28] D. Sheskin, Handbook of Parametric and Nonparametric Statistical Procedures, 2nd ed., Chapman & Hall, CRC, United States of America.
[29] E. Castro, M.T. García-Hernández, A. Gallego, Damage detection in rods by means of wavelet analysis of vibrations: influence of the mode order, J. Sound Vib. 296 (2006) 1028–1038.